Low- and intermediate-energy stopping power of protons and antiprotons in solid targets

C. C. Montanari* and J. E. Miraglia†

Consejo Nacional de Investigaciones Científicas y Técnicas, Universidad de Buenos Aires, Instituto de Astronomía y Física del Espacio, Pabellón IAFE, 1428 Buenos Aires, Argentina

and Universidad de Buenos Aires, Facultad de Ciencias Exactas y Naturales, Departamento de Física, Ciudad Universitaria, 1428 Buenos Aires, Argentina

(Received 4 May 2017; published 25 July 2017)

In this paper we propose a nonperturbative approximation to electronic stopping power based on the central screened potential of a projectile moving in a free-electron gas, by Nagy and Apagyi [Phys. Rev. A **58**, R1653 (1998)]. We used this model to evaluate the energy loss of protons and antiprotons in ten solid targets: Cr, C, Ni, Be, Ti, Si, Al, Ge, Pb, Li, and Rb. They were chosen as *canonicals* because they have reliable Wigner-Seitz radius, $r_s = 1.48$ to 5.31, which cover most of the possible metallic solids. Present low-velocity results agree well with the experimental data for both proton and antiproton impact. Our formalism describes the binary collision of the projectile and one electron of the free-electron gas. It does not include the collective or plasmon excitations, which are important in the intermediate- and high-velocity regime. The distinguishing feature of this contribution is that by using the present model for low to intermediate energies and the Lindhard dielectric formalism for intermediate to high energies, we describe the stopping due to free-electron gas in an extensive energy range. Moreover, by adding the inner-shell contribution using the shellwise local plasma approximation, we are able to describe all the available experimental data in the low-, intermediate-, and high-energy regions.

DOI: 10.1103/PhysRevA.96.012707

I. INTRODUCTION

The energy loss of ions in solids has historically been a subject of interest due to its importance in different fields of technological and biological interest, such as ion-beam analysis, radiation damage, and range of ions in matter. The relevance of this subject can be noted in the extended compilation of experimental data in [1], very active up to the present time.

The theoretical developments cover from the Bethe theory for high energies in the 1930s [2] up to the time-dependent density functional theory for very low impact velocities [3–6], going through the dielectric formalism by Lindhard [7–9] and later models [10–12], the free-electron gas (FEG) models [13,14], and the binary theories [15–18]. Very effective too are the semiempirical descriptions and codes, the most extended of which is SRIM [19]. Many reviews on this subject have been published; see for example the classic ones by Fano [20] and Inokuti [21], or more recently by Arista and Lifschitz [22] and Sigmund [23].

In the last decade, the stopping power has had a revival due to the requirement of more accurate experimental data, and to the possibilities and precision of up-to-date techniques [24]. Perhaps the most challenging ones are the low-energy antiproton experiments at CERN and the future prospects of the Facility for Antiproton and Ion Research [25,26] at Darmstadt.

Based on the publications of experimental works compiled in [1], the number of measured ion-target systems has increased from 74 in the period 2005–2008 to 96 in 2009–2012 and 158 in 2013–2016. The studied targets are approximately two-thirds compounds (mainly oxides and polymers) and one-third atomic targets, with special interest in the very-low-velocity range (i.e., $v < 1$). This revival is related not only to the direct interest in the stopping powers but also to the inclusion of these values in simulations with different purposes [27,28]. It must be mentioned that most of the values included in these simulations come from SRIM [19], or the International Commission on Radiation Units & Measurements reports [29], and important discrepancies have been reported [24,28,30].

The impulse of the new experimental measurements of stopping by low-energy projectiles (i.e., by antiprotons [31–33] and by protons [34–38]) beards the theoretical developments. The expected linear dependence with the velocity, the influence of d-electron excitation, and the density of electrons involved in the projectile loss of energy have attracted many of the stopping power experimental efforts in the last years [39–45]. The theoretical work on low-energy stopping is extensive, such as by the groups of Echenique *et al.* [46,47], Nagy *et al.* [48–50], Arista and coworkers [17,51–53], Cabrera-Trujillo *et al.* [54], and more recently Kadyrov and coworkers [18,55] and Grande [56].

The accuracy of the new experimental techniques and the necessity of full theoretical data lead us to wonder what is the highest theoretical precision to describe these low-energy new experimental measurements. For this purpose, we present here a nonperturbative binary collisional model to describe the electronic stopping power dS/dx of heavy charged projectiles in a FEG. The description at low impact velocities v is amplified by calculating the friction parameter $Q = (dS/dx)/v$. In order to have a clear view of the problem to solve, we analyze the case of protons and antiprotons (no charge state considerations) and targets of well-established Wigner-Seitz radius, r_s.

We define *the canonical* metallic solids as those of reliable r_S, thus any doubts arising from their description can be dispelled. The criterion we followed is that the theoretical r_S obtained considering the atomic density and the number of valence electrons do not defer more than 5% with respect

*mclaudia@iafe.uba.ar
†miraglia@iafe.uba.ar

to the value deduced from the experimental plasmon energy [57]. In this way, we state these *canonical* targets as settings for future theoretical and experimental comparisons.

The present model is based on the central screened potential of a projectile moving in a free-electron gas, by Nagy and Apagyi [48], corrected in order to verify the cusp condition. Thus, we have successfully faced the theoretical problem of negative induced density by negative charge intruders [58].

The main characteristics of our proposal are (i) the use of a central potential $V_Z(r)$ that is Coulombic at the origin and decays exponentially at large distances; (ii) an induced density that verifies the closure relation, which is finite at the origin and never becomes negative (as happens if we use the Yukawa potential); and (iii) the cusp condition is imposed through an additional parameter λ. This strategy is valid at low energies, or at least where plasmons play a minor role. It only accounts for the outer electrons, so that inner-shell contributions have to be included in an independent form.

The goal of this paper is to describe the stopping power of ions in solids in an extended energy region. For this purpose, we resort to two different descriptions for the valence electron contribution: the present binary nonperturbative model for low and intermediate energies, and the perturbative dielectric formalism in the intermediate- to high-energy region. The dielectric formalism is perturbative but contains not only binary but also collective excitations. The inner-shell contribution is included by using the proved shellwise local plasma approximation (SLPA) [11,59,60].

We chose ten canonical targets, Cr, C, Be, Ti, Si, Al, Ge, Pb, Li, and Rb, of Wigner-Seitz radius $r_S = 1.48$–5.31, covering most of the metallic solids. These targets belong to the groups of alkaline metals (Li, Rb, Be), the post-transition metals (Al, C, Si, Ge, Pb), and the first groups of the transition metals (Ti and Cr). Among the transition metals, those elements with few d electrons also have well-established r_s values (groups 3 to 6 of the periodic table of elements). Instead, we skip here groups 7 to 12, where d electrons play a quasi-FEG role depending on the impact velocity. There are very interesting targets that have been an object of extensive experimental research in the last decade, focused on targets such as Pd, Pt, Cu, Ag, Cu, Au, or Zn [39–45].

In this paper we only consider targets for which there are low-energy experimental data in the literature. For proton impact we use the compilation in [1], and for antiproton impact we use the measurements by Møller and collaborators [31–33].

We describe the present formalism in Sec. II. In Sec. III we show the scope of the model by comparing it with the low-energy measurements for protons and antiprotons. We extend the theoretical-experimental comparison from 0.25 to 500 keV by combining the binary and the dielectric formalisms for the FEG, and the SLPA for the inner shells. The experimental needs and future prospects are discussed in Sec. IV. Atomic units are used in all this paper, except when it is explicitly stated.

II. THEORY

A. Potential and density

Consider a heavy bare Coulomb projectile of charge Z and velocity v traveling within a FEG. Let us model the projectile-electron interaction by means of the central effective potential $V_Z(r)$ introduced by Nagy and Apagyi [48]:

$$V_Z(r) = -\frac{Z}{r}(V_1 e^{-\mu_1 r} + V_2 e^{-\mu_2 r}), \tag{1}$$

with

$$V_1 = \frac{(\alpha+\beta)^2}{4\alpha\beta}, \quad \mu_1 = \alpha - \beta$$

$$V_2 = -\frac{(\alpha-\beta)^2}{4\alpha\beta}, \quad \mu_2 = \alpha + \beta.$$

This screened potential tends exponentially to zero at large distances and has the correct limit $V_Z(r) \to -Z/r$ as $r \to 0$ for any value of α and β.

The induced density n_i can be determined by using the Poisson equation to get

$$n_i(r) = Z\,\frac{(\alpha^2-\beta^2)^2}{16\pi\alpha\beta\, r}(e^{-\mu_1 r} - e^{-\mu_2 r}). \tag{2}$$

It can be easily checked that n_i verifies the desired closure relation

$$\int d\vec{r}\; n_i(r) = Z, \tag{3}$$

as far as $\mathrm{Re}(\alpha+\beta) > 0$, and that it is finite at $r = 0$:

$$n_i(r) = \frac{Z}{8\pi}(\alpha^2-\beta^2)^2\left(\frac{1}{\alpha} - r\right) + O(r^2). \tag{4}$$

Following Nagy and Echenique [61], the parameters α and β are defined as

$$\alpha = \sqrt{b/\lambda + \omega_P/\sqrt{\lambda}}, \tag{5}$$

$$\beta = \sqrt{b/\lambda - \omega_P/\sqrt{\lambda}}, \tag{6}$$

where b can be related to the real part of the Lindhard dielectric function:

$$b = \frac{v_F^2/3}{\frac{1}{2} + \frac{v_F^2 - v^2}{4v\,v_F}\ln\left|\frac{v+v_F}{v-v_F}\right|}, \tag{7}$$

with v_F being the Fermi velocity, $v_F = 1.917\, r_S^{-1}$, and $\omega_P = 1.732\, r_S^{-3/2}$ is the plasmon frequency. As in [61], we leave λ as a free parameter determined by imposing the cusp condition to the density:

$$-2Z = \lim_{r\to 0}\frac{\frac{d}{dr}n_i(r)}{n_i(r) + n_0}. \tag{8}$$

Note that Eq. (7) introduces the dependency of the potential with the ion velocity. The asymptotic limits of Eq. (7) are

$$b \to \begin{cases} v_F^2/3, & \text{as } v \to 0 \\ v^2, & \text{as } v \to \infty \end{cases}. \tag{9}$$

The cusp condition greatly improves the behavior of n_i at the origin, erasing nonphysical negative electronic densities. For example, in the case of antiprotons at rest in a FEG, $\lambda = 1$ gives negative density and $n_i(0) + n_0 < 0$, for certain values of r_S. Instead, by imposing the cusp condition (8) to get λ, very reasonable values are obtained, i.e., $-n_0 < n_i(0) < n_0$.

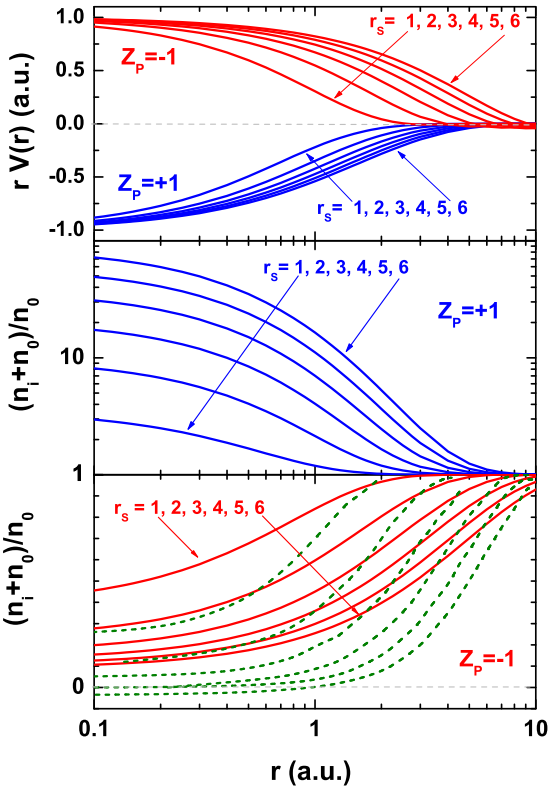

FIG. 1. Screening potentials and electronic densities generated by protons ($Z_P = +1$) and antiprotons ($Z_P = -1$) at rest in a FEG. We display these for different values of $r_S = 1$–6 as indicated inside the figure. Curves: Solid lines denote present results, which verify the cusp condition at the origin and have positive densities for any value of r_S; dashed lines denote the results for antiprotons in a FEG by Singwi *et al.* [58].

It is worth mentioning that, no matter the impact velocity, the electronic density always verifies the cusp condition at the origin.

In Fig. 1 we plotted the potentials and total electronic densities (solid lines) generated by protons ($Z = +1$) and antiprotons ($Z = -1$) at rest. We consider r_S ranging from 1 to 6, which covers by far all the known values. As expected, the potential tends to be Coulombic as r_S increases (the density of electrons decreases, and therefore the screening too). The induced densities displayed in Fig. 1 satisfy the cusp condition imposed by λ. As can be noted, even the densities originated by antiprotons never become negative. The shape of the density induced by a negative charge can also be interpreted as a pair distribution function. For the sake of comparison, we include in Fig. 1 the pair distribution function reported by Singwi *et al.* [58]. It is the best random-phase approximation (RPA), including short-range correlation and exchange effect. Even so, this RPA pair distribution function presents negative densities at the origin for $r_S > 4$.

At high velocities ($v \gg v_F$), $\lambda \to 1$, and the following expected limits are verified:

$$V(r) \underset{v\to\infty}{\to} -\frac{Z}{r}\, e^{-\frac{\omega_P}{v} r} \tag{10}$$

and

$$n_i(r=0) + n_0 \underset{v\to\infty}{\to} n_0 \left(1 + 2\,\frac{Z}{v}\right). \tag{11}$$

Beyond the theoretical validity of these limits, the physics involved in the present model only describes binary collisional processes. The collective electronic excitations, also known as plasmon excitations, are not included. The plasmon contribution is important at high energies. Within the dielectric formalism, the minimum impact velocity v_P to excite plasmons can be approximated as [62]

$$v_P/v_F \simeq 1 + (3\pi\, v_F)^{-1/2}. \tag{12}$$

We will return to this point in Sec. III where we compare our results (using the present nonperturbative model and using the Lindhard dielectric formalism) to the existing experimental data.

B. Stopping power and friction

The calculation of stopping power, or energy loss per unit path length, dS/dx, implies the integration of the electron momentum $\vec{k}_i$ over all the Fermi sphere [13]:

$$\frac{dS}{dx}(v) = 2\int \frac{d\vec{k}_i}{(2\pi)^3}\,\theta(k_i - k_F)\,\frac{ds}{dx}(\vec{k}_i') \tag{13}$$

with

$$\frac{ds}{dx}(\vec{k}_i') = 2\pi\,\frac{k_i'}{v}\,\vec{k}_i'\cdot\vec{v}\;\sigma_{\rm tr}(\vec{k}_i') \tag{14}$$

and $\vec{k}_i' = \vec{k}_i - \vec{v}$ the relative velocity. The transport cross section $\sigma_{\rm tr}(k)$ is

$$\sigma_{\rm tr}(k) = \frac{4\pi}{k^2}\sum_{l=0}^{\infty}(l+1)\sin^2\left[\delta_l(k) - \delta_{l+1}(k)\right] \tag{15}$$

with $\delta_l(k)$ being the phase shifts generated by the potential $V_Z(r)$. The central potential given by Eq. (1) is expressed in terms of exponentials, so the first Born approximation to $\sigma_{\rm tr}(k)$ can be calculated straightforwardly.

An alternative expression to the transport cross section has been recently proposed by Grande [56], derived from the retarding force due to an asymmetrically induced charge density acting on the projectile. This noncentral density is calculated from the spherically symmetric potential using the partial-wave expansion in a frame fixed to the ion. The results by Grande are interesting, mainly in the intermediate-energy region, which is the conflictive zone where the validities of the high-energy models (including plasmons) and the low-energy ones (binary) compete.

The stopping power can also be expressed in terms of the friction parameter $Q_Z(v)$ as

$$\frac{dS}{dx} = Z^2\, v\, Q_Z(v). \tag{16}$$

According to Fermi and Teller [63], at low impact velocities the stopping power is expected to show a linear dependency with the velocity, and so $Q_Z(v)$ tends to a constant. In the perturbative regime the stopping power is proportional to Z^2, so $Q_Z(v)$ is independent of Z.

The linear-response theory (LRT) by Ferrell and Ritchie [13] predicts

$$Q^{\mathrm{LRT}}(v \to 0) = \frac{2}{3\pi}\left[\ln\left(1+\frac{6.03}{r_S}\right) - \frac{1}{1+\frac{r_S}{6.03}}\right]. \quad (17)$$

This is a first perturbative approximation, and therefore insensitive to the charge Z of the intruder.

Taking into account the projectile charge and velocity and the screening by the FEG, a reasonable criterion for the perturbative regime is

$$v/v_F \geqslant Z_P\, r_S. \quad (18)$$

In fact, as $v_F = 1.917/r_S$, this criterion is equivalent to $v \geqslant 1.917\, Z_P$. We will return to this in the next section in view of the theoretical-experimental comparison.

III. RESULTS AND COMPARISON WITH THE EXPERIMENTAL DATA

In this section we display the results of the present formalism for antiproton and proton impact in Cr, C, Be, Ti, Si, Al, Ge, Pb, Li, and Rb. We chose them because they are typical canonical metals, i.e., their valence electrons act as a free-electron gas of a constant and well-known value of r_S. As we will comment later in this paper, there are many more metallic targets that could be described using the present model, but there are no experimental measurements at low energies to compare with (see Sec. IV).

In Table I we list the ten targets, their r_S and v_F values [57], the calculated v_P [62], and our nonperturbative results for $Q_{+1}(v)$ and $Q_{-1}(v)$ in the limit $v \to 0$. These values may be used as predictions for future low-energy measurements by proton and antiproton impact.

A. Proton and antiproton energy loss at low impact velocities

In what follows we compare our friction $Q_Z(v)$ at low impact energies with the experimental data available in the literature. We focus on this energy region in order to have only the contribution of the valence electrons. In Fig. 2 we report

TABLE I. The ten solid targets studied here, their Wigner-Seitz radii r_S and Fermi velocity v_F [57], the calculated minimum velocity for plasmon excitation v_P given by Eq. (12), and the present results for the friction in the limit $v \to 0$ for proton $Q_{+1}(0)$ and antiproton $Q_{-1}(0)$ impact, as defined in Eq. (16). Atomic units are used throughout this table.

	r_S	r_S^{exp}	v_F	v_P/v_F	$Q_{+1}(0)$	$Q_{-1}(0)$
Cr	1.48	1.55	1.30	1.29	0.307	0.176
C	1.60	1.66	1.20	1.30	0.295	0.163
Be	1.87	1.78	1.03	1.32	0.269	0.141
Ti	1.92	1.93	1.00	1.33	0.264	0.137
Si	2.01	1.97	0.955	1.33	0.256	0.131
Al	2.07	2.12	0.927	1.34	0.250	0.127
Ge	2.09	2.02	0.918	1.34	0.248	0.126
Pb	2.30	2.26	0.834	1.36	0.229	0.113
Li	3.27	3.21	0.587	1.43	0.150	0.075
Rb	5.31	5.45	0.361	1.54	0.041	0.048

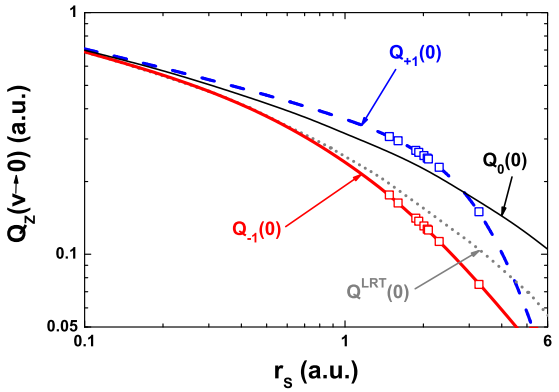

FIG. 2. The friction in the limit $v \to 0$, as a function of r_S. Curves: The solid red line denotes present results for antiprotons, Q_{-1}; the dashed blue line denotes present results for protons, Q_{+1}; the thin black line denotes Q_0 given by Eq. (19); and the gray dotted line denotes $Q^{\mathrm{LRT}}(v)$ in the linear-response theory by Ferrel and Ritchie [13] given by Eq. (17). Symbols: Hollow squares are the theoretical values displayed in Table I for specific targets.

our results for proton Q_{+1}, and for antiproton impact Q_{-1}, in the limit $v \to 0$ as a function of r_S. The theoretical values displayed in Table I for specific targets are also included in Fig. 2. These results confirm the experimental evidence that protons cede more energy to the FEG than antiprotons.

We also include in Fig. 2 (dotted line) the prediction of the LRT by Ferrell and Ritchie [13], Eq. (17), which is independent of the projectile charge. The comparison of our nonperturbative values and the linear ones is very interesting. Our results correctly tend to the Q_{LRT} as $r_s \to 0$, where we can consider that the screening of the projectile is so high that it can be described as a perturbation. In contrast, as r_S increases, the projectile becomes a huge perturbation to the FEG so the linear models cannot describe it.

To explore the perturbative limit we also calculated the friction for $Z \to 0$,

$$Q_0(v) = \lim_{Z\to 0} Q_Z(v), \quad (19)$$

and plotted it in Fig. 2 (black solid line). For $r_S > 1$, Q_0 divides the region between Q_{+1} and Q_{-1}, the known Barkas effect [65].

The description of the energy loss by antiproton impact is a challenge for any model, but it has the advantage that there is no possibility of charge exchange [25]. The measurements by Møller *et al.* [31–33] for antiprotons in several targets allowed us to test our theory with the Coulomb sign of the intruder. In Fig. 3 we display the present values for the friction as a function of the impact velocity for antiprotons in C, Si, and Al. Note that the agreement is very good in a linear-scale plot. We focused on the low-velocity region in order to have only the valence electron contribution. Inner shells, however, may be contributing for Al above $v = 1.5$. The theoretical description of low-energy antiproton measurements is an open path for future experimental research [25]. Energy-loss investigation is part of the physics program of the next-generation antiproton source FLAIR (Facility for Low-Energy Antiproton and Ion Research) [64], planned for the next five years.

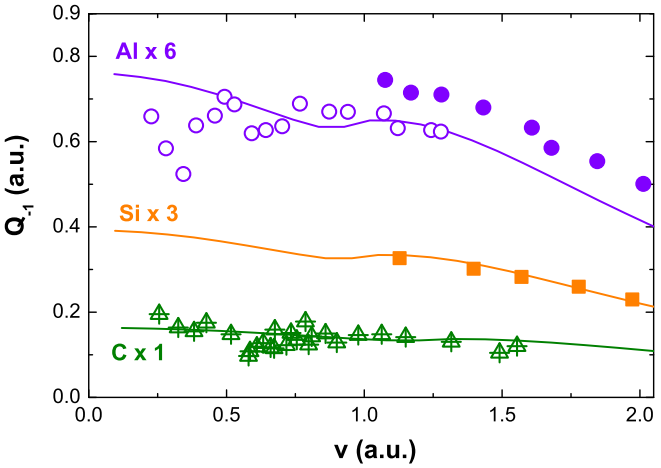

FIG. 3. The friction parameter Q_Z as a function of the impact velocity for antiprotons in C, Si, and Al. Curves denote present nonperturbative results. Symbols denote experimental data: for Al, empty circles [31] and solid circles [33]; for Si, solid squares [33]; and for C, crossed triangles [32].

At low impact energies the stopping power depends only on the value of r_S, so it should be the same for different metals of similar r_S. In Fig. 4 we plot together the experimental data for protons in three targets of $r_S \simeq 2$, Al, Ge, and Si. As can be noted in this figure, all the low-energy measurements are quite close within the experimental spread. We also display in this figure our theoretical results for Al, Si, and Ge, which are actually very close and nicely describe the low-energy measurements in the three targets. This confirms that r_S is the *only* relevant parameter at low energies.

The experimental frictions displayed in Fig. 4 are $Q_{+1}^{\rm exp} = 0.25 \pm 0.07$, and so are our theoretical results, with $Q_{+1} \to 0.25$ as $v \to 0$. Similar values of the friction at low energies are expected for other metals of $r_S \simeq 2$, such as Zn, Ga, or Te. The recent low-energy measurements for protons in Zn [43] confirm this, but the most interesting point is the prediction of the value of Q_{+1} for future measurements in Te, with no data of stopping at all, or in Ga, with no low-energy measurements [1].

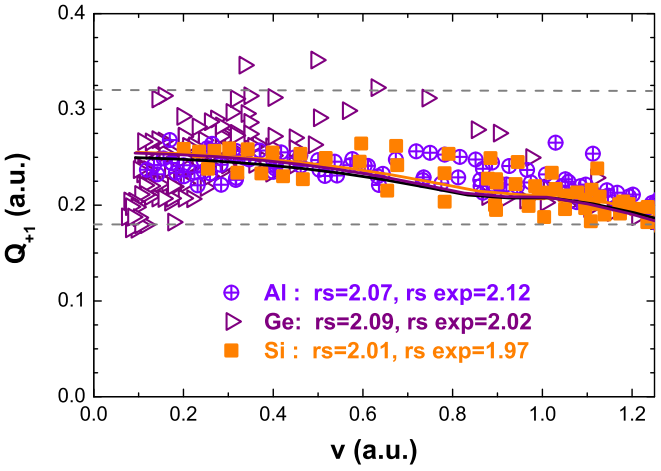

FIG. 4. The friction parameter Q as a function of the impact velocity for protons in Ge, Al, and Si. Curves denote present nonperturbative results. Symbols denote experimental data available as compiled in [1].

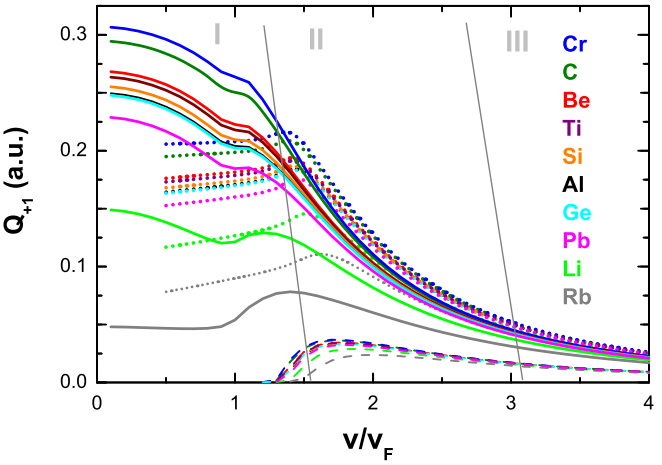

FIG. 5. Friction for protons in different targets as a function of the ratio of the impact velocity and the Fermi velocity. Curves: Solid lines denote the present nonperturbative results; dotted lines denote the Lindhard dielectric formalism results; dashed lines denote the isolated plasmon excitation contribution included in the calculations using the dielectric formalism. The different targets are plotted in the following order: from top to bottom, Cr, C, Be, Ti, Al, Si, Ge, Li, and Rb.

B. Low- to intermediate-energy region

Above a certain impact velocity v_P, the energy loss implies not only binary but also collective excitations (plasmons) [13]. Though the present nonlinear binary theory has the correct high-energy limit, in the intermediate-energy region it lacks the collective contribution. The extension to impact velocities $v > v_P$ can be performed by using the well-known Lindhard dielectric formalism [7,8]. This formalism includes both binary and collective excitations, and tends to the Bethe limit at high energies, but it is a linear-response approximation, and therefore valid within the perturbative limits.

A detailed comparison of the friction as a function of the impact velocity by using the present model (nonperturbative) and the Lindhard dielectric formalism (perturbative) is presented in Fig. 5. The results for protons in Cr, C, Be, Ti, Si, Al, Ge, Pb, Li, and Rb are displayed in this figure from top to bottom. Note that the lower the r_S the larger stopping power. Three regions, I, II, and III, are indicated in Fig. 5, separated at v_P and $2\ v_P$. In region I ($v < v_P$), the present collisional formalism (solid lines) is very appropriate because it includes all the perturbative orders and only binary collisions are involved. Instead, the dielectric formalism (dotted lines) is very poor; it underestimates stopping power in this region. In contrast, in region III ($v > 2\ v_P$), which is clearly perturbative, the dielectric formalism is correct since it includes both plasmons and single-electron excitations. The nonperturbative results are below the dielectric ones in this region. Region II is the intermediate one, in which nonlinear effects and plasmon contribution compete in importance. The validity of each

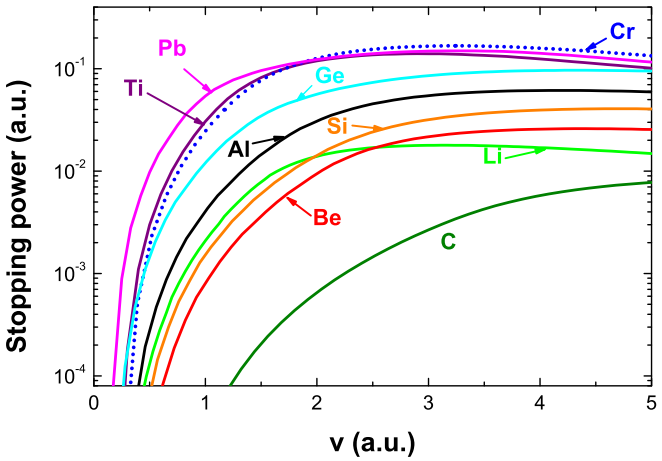

FIG. 6. Inner-shell contribution to the stopping power of protons in Cr, Pb, Ti, Ge, Al, Si, Li, Be, and C, as a function of the impact velocity. Curves denote results obtained with the SLPA considered from the K shell to the subvalence shell, according to each target [11,59,60].

formalism in this region is subject to the comparison with the experimental data, as will be shown in Sec. III D.

We also include in Fig. 5 the isolated plasmon contribution (dashed lines). Note that the impact velocity v_P above which the plasmon excitation starts contributing agrees quite well with the values in Table I. It can be observed that for $v > v_P$ plasmon excitation is not negligible at all. As predicted by Lindhard and Winter [8], at very high energies the equipartition rule holds and the binary stopping equals to the plasmon one.

C. Extension to higher energies: The inner-shell contribution

At sufficiently high impact energies the impinging projectile will be able to remove subvalence electrons. To extend the theoretical description to intermediate and high velocities we include the inner-shell contribution by resorting to the SLPA [11,59,60]. During the last years we have developed this model based on the dielectric formalism and the local plasma approximation by Lindhard and Scharff [9]. The contribution of each subshell of target electrons is described including screening, collective response, and correlation in the final state. The inputs are the densities and binding energies of each subshell. For nonrelativistic atoms, i.e., atomic numbers up to 54, they can be obtained from the Hartree-Fock wave functions by Bunge *et al.* [66]. For targets of higher atomic numbers, the relativistic Dirac equation must be solved. The most interesting characteristic of the SLPA is that it is a density-based model, and therefore capable of being used for molecular targets as far as a good description of the different shells' electronic density is available [67,68]. The great limitation is that it is a perturbative model.

In Fig. 6 we display the SLPA results for the stopping power due to the inner shells of Cr, C, Be, Ti, Al, Si, Ge, Li, and Pb. For Pb ($Z = 82$, relativistic target) we used the results obtained by employing the GRASP code in [60]. For the rest, we used the atomic wave functions by Bunge *et al.* [66]. As we are dealing with solids, the binding energies are slightly different from those of the gas phase. We use the experimental binding energies relative to the top of the Fermi level for metals compiled by Williams [69], instead of the theoretical values for single atoms, which correspond to gases.

It can be noted in Fig. 6 that the inner-shell contribution falls down several orders of magnitude when going from high to low energies. We are fully aware of the inability of the perturbative SLPA to describe the low-energy region, but inner-shell contribution is relatively negligible in this energy region. In contrast, as velocity increases, the relative importance of the inner shells grows and, at the same time, the validity of the SLPA starts to hold.

D. Comparison with the experiments in an extended energy range

We performed an extensive comparison of the present theoretical results and the experimental data in the IAEA database [1]. We analyzed the stopping of protons in Cr, C, Be, Ti, Si, Al, Ge, Pb, and Li. We did not include Rb in this comparison because there are no measurements in the low-energy region, which is our main interest. By combining our nonperturbative and perturbative calculations in different energy regions, we managed to cover an extended range of (0.25–500) keV. The extension to higher impact energies by using the dielectric formalism and the SLPA has already been demonstrated [11,59,60].

In Figs. 7–9 we compare our theoretical results with the available experimental data [1] for the nine targets mentioned above. We display the friction for the lowest velocities in order to heighten the low stopping values. Instead, for the highest velocities we plotted the stopping power.

We show in these three figures the total values using the nonperturbative approximation for the FEG (red solid lines) and the perturbative model for the FEG (blue dashed lines). The total stopping power was obtained by adding the SLPA results for the inner-shell contribution. The experimental data in Figs. 7–9 follow the same notation using different letters as symbols as in [1].

We separate three regions as in Fig. 5. Both boundaries, at v_P and 2 v_P, are displayed with vertical dashed lines. These energy regions involve different physical regimes. In the low-energy region I, valence electrons are the main contribution and a nonperturbative description is mandatory. The high-energy region III corresponds to the perturbative regime. As mentioned before, the intermediate region II is very interesting because plasmon excitation starts to occur and the validity of the perturbative description will depend on each case. It is worthwhile to note that the stopping maximum is in this region, for impact velocity $v \gtrsim v_P$.

Figure 7 displays the present results for Cr, C, and Be ($r_S = 1.48, 1.6$, and 1.87, respectively). In the upper plot, for protons in Cr, our nonperturbative results clearly describe the experimental measurements in the whole energy range. The data by Eppacher and Semrad [70] of 1992 (represented by letter "F" in this plot) are the most recent ones and cover an extended energy region from 20 to 700 keV. Only the low-energy values, i.e., impact velocity below 1.2, seem to be too large. There are no experimental data for $v < 1$. New low-energy measurements for this system are welcome. On the other hand, the FEG of Cr has the highest electronic

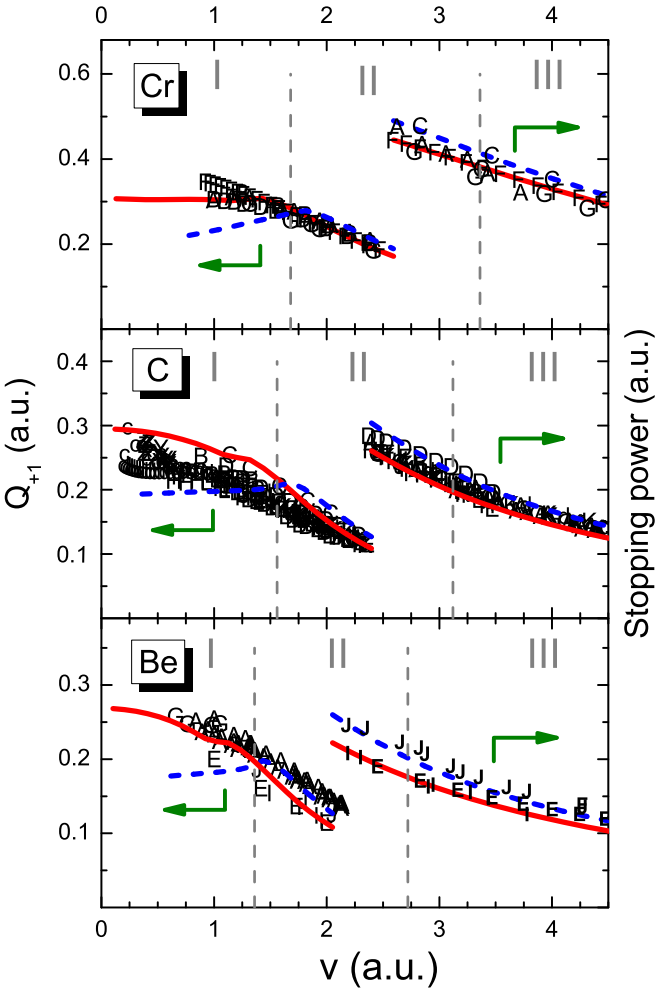

FIG. 7. Total friction ($v < 1.5\ v_P$) and stopping power ($v > 1.5\ v_P$) (including FEG and inner shells) as a function of the impact velocity, for protons in Cr, C, and Be. Curves: Red solid lines denote present results using the nonperturbative model for the FEG; blue dashed lines denote present values using the Lindhard dielectric function for the FEG (linear response). In both cases the inner-shell contribution is included, calculated with the SLPA [11]. Letters denote available experimental data in [1] and references therein.

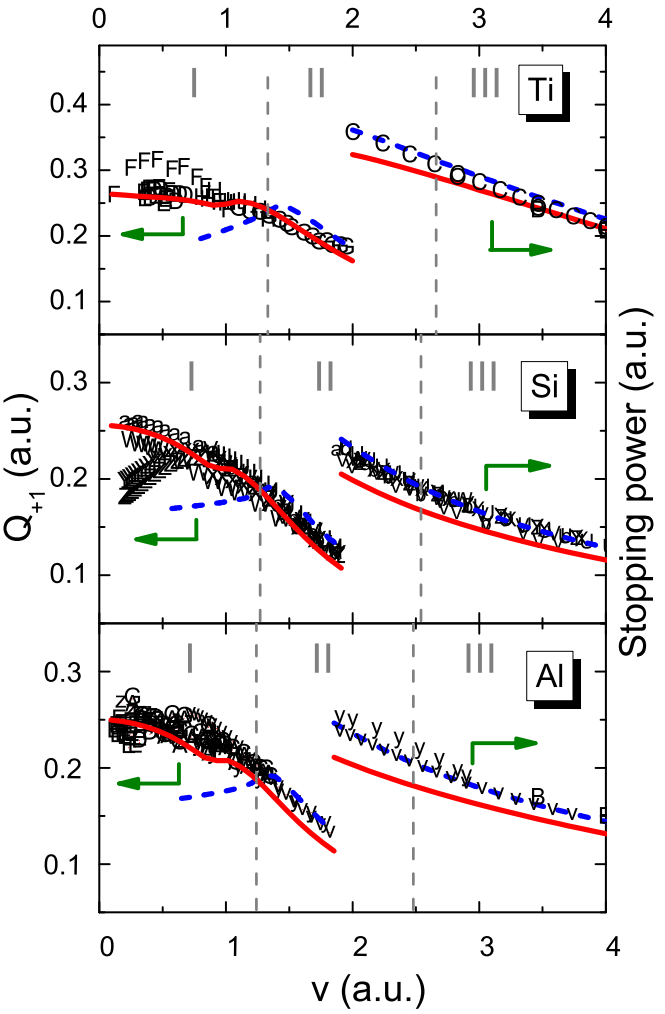

FIG. 8. Total friction ($v < 1.5\ v_P$) and total stopping power ($v > 1.5\ v_P$) (including FEG and inner shells) as a function of the impact velocity, for protons in Ti, Si, and Al. Curves and symbols are as in Fig. 7. For Si and Al the whole available data in [1] are abundant. We only include here the data since 1990. We added recent data for H in Al by Møller *et al.* [31] (letter G), that was not in [1].

density, or equivalently the smallest r_S considered here. This implies a large screening of the projectile, and almost a perturbative regime in the whole velocity range. This explains the agreement of the perturbative calculations down to impact velocities $v \geqslant 1.7$.

Also displayed in Fig. 7 are the present results for stopping of protons in amorphous carbon. This is one of the targets with more experimental measurements due to its different applications. However, the complexity of carbon (amorphous or crystal phases) also introduces dispersion among different sets of measurements. We show in this figure the available data since 1980. It can be noted that our nonperturbative friction reproduces the experiments in regions II and III, but overestimates a little in region I. As predicted, the perturbative results are reasonable for $v \geqslant 1.917\ Z_P$. Note that for carbon we also reproduce very well the antiproton impact measurements, even for very low velocities (see Fig. 3).

Finally, for beryllium, at the bottom part of Fig. 7, we begin to note the difference between the nonperturbative and the perturbative descriptions, the latter including plasmons. The separation between the curves is clear for $v > v_P$. The agreement of the present nonperturbative results with the low-energy data is very good. However, for $v \geqslant 1.5$ the nonperturbative results are too low, while the perturbative ones describe well the experiments. This difference is explained by the lack of plasmon contribution in the binary model. The experimental values represented by letters "E" and "I" correspond to the measurements by Warshaw [71] and by Kahn [72] in the 1950s, which are below the general tendency of much recent data [1]. It can be said that the combination of the present nonperturbative model for $v \leqslant v_P$ and the dielectric formalism for $v \geqslant v_P$ gives a good description of the energy loss of protons in Be in the whole energy range.

Figure 8 displays the present results for Ti, Si, and Al. Again the vertical dashed lines separate the three energy regions mentioned above. In the upper figure, the energy loss in Ti

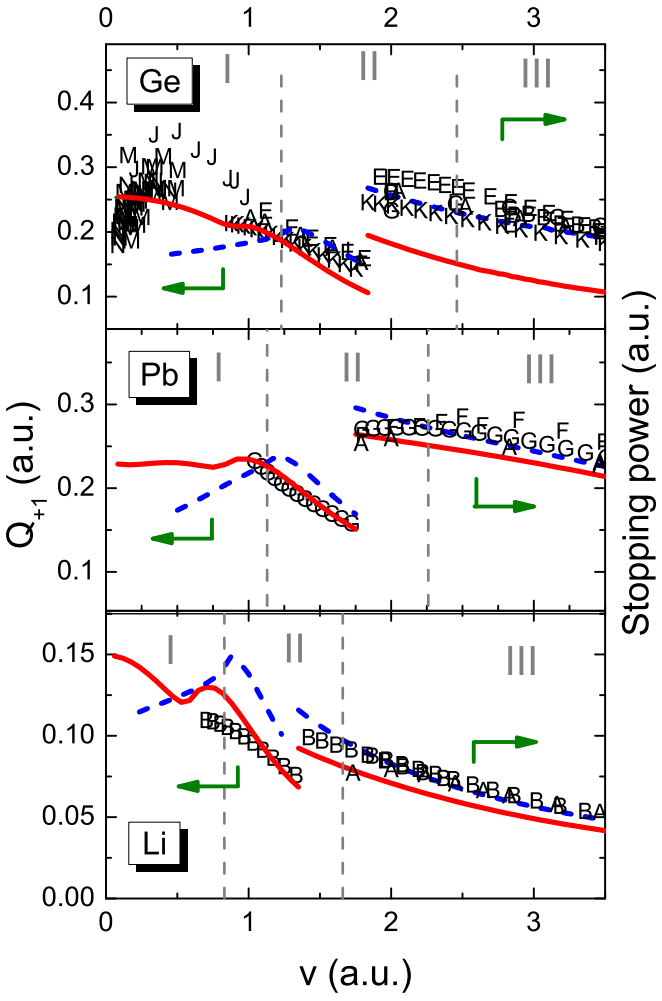

FIG. 9. Total friction ($v < 1.5\, v_P$) and total stopping power ($v > 1.5\, v_P$) (including FEG and inner shells) as a function of the impact velocity, for protons in Ge, Pb, and Li. Curves and symbols are as in Fig. 7.

is nicely described in the whole energy range, showing a very good agreement with the experiments. For low velocities, $v < 1.8$ a.u., the present nonperturbative formalism describes the data correctly. Only the low-energy measurements by Arkhipov and Gott in 1969 [73] (letter "F") are higher than the rest. This detail would not be noticed if we plotted the stopping power instead of the friction coefficient at low energies. Some doubts on the normalization of Arkhipov and Gott's data have been stated by Paul in [1]. Titanium is a target of technological importance that deserves new stopping measurements, not only in the low-energy region but also around the stopping maximum, where only one set of data is available (by Ormrod in 1971 [74], letter "G" in this figure). In the intermediate region II, the binary model clearly underestimates the experimental values for $v \geqslant 2$. This can be adjudicated to the lack of plasmons, included in the dielectric formalism.

The energy loss of protons in Si has more than 600 experimental values for the different energies. Among all these data, we show in Fig. 8 those measured since 1990. It is a criterion to have a clearer view of the experimental tendency and to avoid the great dispersion among the oldest measurements. The agreement of our results for protons in Si shown in Fig. 8 is very good from the very low to the high energies. This is more noticeable if we focus on the latest experimental measurements: the low-energy data by Hobler *et al.* in 2006 [35] (letter "a" in region I), by Fama *et al.* in 2002 [36] (letter "W" in regions I and II), and the high-energy data by Abdesselam *et al.* in 2008 [75] (letter "b" in regions II and III). Instead, the measurements by Konac *et al.* in 1998 [76] (letters "Y" and "Z") are too low for $v < 0.7$. Again this difference in the friction would be very small if we plot the stopping power in the low-velocity regime too. The friction plot acts as a magnifier of the low-velocity behavior, which is very demanding for any theoretical description. We describe Si as a free-electron gas with no energy gap, and we do not extend the calculations below $v = 0.1$. We do not discuss here the threshold of the Si as semiconductor [37,77], which is below $v = 0.03$. For $v > v_P$ the perturbative calculation improves the binary one. The combination of formalisms, the nonperturbative one in region I and the dielectric one in regions II and III, leads us to correctly describe the experimental data of stopping power of protons in Si in the whole energy range. This includes the stopping maximum, which is around 52 keV ($v = 1.5$). For Si, we obtain very good agreement with the experiments, not only for protons (Fig. 8) but also for antiprotons (Fig. 3).

In the bottom plot of Fig. 8 we display the theoretical-experimental comparison for aluminum, which is one of the most studied targets. As for the previous case, we restrain the comparison to modern experiments (1990 up to now). The agreement at low energies is quite nice, especially with the newest low-energy data by Primetzhofer *et al.* [38] in 2011 (with letters "E" and "D" in Fig. 8). Clearly the perturbative model underestimates the friction in this region. The results in regions II and III show that for $v > v_P$ the nonperturbative formalism (binary) underestimates the measurements, while the dielectric results (binary and plasmons) nicely describe the data. Our proposal is that the combination of both models allows one to describe the stopping of H in Al in the whole energy range, from the very low up to the high energies.

Finally, in Fig. 9 we plot the energy loss of protons in Ge, Pb, and Li. We can note in these cases that all the physics involved is enhanced, i.e., the importance of a nonlinear description as compared to the contribution of plasmons. For the case of Ge, in the upper part of Fig. 9, the validity ranges of the nonperturbative binary formalism and the dielectric formalism (binary and plasmons) are very clear. The description of the experimental data by the nonperturbative calculation in region I is quite good. It nicely links the data by Eppacher and Semrad [70], (with letter "K"), and the most recent measurements (letters "N" and "M") by Bauer and collaborators in Linz [37]. On the other hand, the data by Arkhipov and Gott in 1969 [73] (letter "J") is clearly above the rest. Present results also agree with the time-dependent density functional theory values for protons in Ge [78], which apply only to very low energies (i.e., $v \leqslant 0.6$). In regions II and III, our binary formalism underestimates the measurements showing the importance of plasmon excitations in these energy regions. Instead, the perturbative results describe nicely the measurements for $v > v_P$, and clearly separate from the binary results. This

behavior is the expected one; it has been already found for Si and Al in Fig. 8, but for Ge the difference is more pronounced.

The medium graphic in Fig. 9 corresponds to protons in Pb. This case is special because we are dealing with a relativistic target, 82 bound electrons, including the K-L-M-N-O shells and the $6s^2$-$6p^2$ electrons as free-electron gas. We follow [60] to calculate the inner-shell contribution to the energy loss by using the SLPA together with the relativistic densities of electrons of each subshell (spin-orbit split) obtained with the GRASP code. In the present calculations, the experimental binding energies were used [69]. This improves our previous results in [60] in the high-energy region.

The $r_S = 2.3$ of Pb is higher than in the previous targets, hence it is more nonperturbative. This can be noted in the comparison of both models (solid and dashed curves) in the intermediate region II. We can say that the nonlinear contributions are more important than the plasmons for Pb. The binary nonperturbative calculations for Pb clearly improve the perturbative ones for $v \leqslant 1.5\, v_P$, with very good agreement with the Eppacher and Semrad data [70]. Unfortunately, there are no measurements of stopping of protons in lead below 25 keV. Our results indicate an almost linear tendency of the stopping of protons in Pb for $v \leqslant 0.7$, with $Q_{+1} \sim 0.23$. Low-energy measurements would be a good test for this prediction.

Finally, we display in the bottom part of Fig. 9 our results and the experimental data for protons in Li. This is the target with the largest value of $r_S = 3.27$ we here considered, and so the smallest electron density and the lowest Fermi velocity, $v_F = 0.59$. This makes Li a very interesting test of our model because it is highly nonperturbative around the stopping maximum, i.e., between 20 and 40 keV. Only two sets of data are available for this system [1], so more measurements are welcome, mainly for $v < 1.5$. The present nonperturbative model describes properly the experimental values in the intermediate region II, but it overestimates the data for $v < 1$. It is worthwhile to mention that different theoretical calculations for H in solid Li by Kaneko [79] and by Cabrera-Trujillo *et al.* [80] are also above the measurements by Eppacher *et al.* [81] around the stopping maximum. In the high-energy region III, the perturbative model is valid, and the good description of the experiments for impact velocities $v > 1.7$ shows the importance of plasmon excitations.

IV. EXPERIMENTAL SCARCITY AND FUTURE PROSPECTS

The great absence in the comparisons of Sec. III D is rubidium, with a FEG characterized by $r_S = 5.31$ and a very low Fermi velocity, $v_F = 0.361$. Protons introduce a huge perturbation to such a FEG, which can test any nonperturbative theoretical model to the limit. Unfortunately, the available measurements are for $v \geqslant 1.1$, which is three times v_F. This makes Rb a very interesting target to be studied, experimentally and theoretically, and an opportunity of future research.

We expect the predictions for low-velocity friction as a function of the r_S presented here (Fig. 2 and Table I) to be benchmarks for future measurements. There are more canonical metals [57]. In general, these targets belong to the s and p blocks of the periodic table of elements (alkaline metals and earth metals with valence s electrons, post-transition metals, and metalloids, with valence p electrons). However, for many of them there are no experimental stopping powers at low impact energies. For example, for proton impact in the s-block elements there are no data for impact energies $E < 20$ keV for Mg ($r_S = 2.66$), Ca ($r_S = 3.27$), and Sr ($r_S = 3.59$), and there are no data at all for Na ($r_S = 3.99$). Also some relativistic targets, such as Cs ($r_S = 5.75$) and Ba ($r_S = 3.74$), have no stopping data at all. Among the elements of the p block of metals, there are no low-energy data for protons in Ga ($r_S = 2.19$) for $E < 70$ keV, in Sn ($r_S = 2.4$) for $E < 20$ keV, and there are no data at any impact energy for protons in Se ($r_S = 1.84$) and Te ($r_S = 2.09$). Note that the latter is a very interesting case to test the universal predictions of Fig. 4 for the $r_S \simeq 2$ elements.

The transition metals of groups 7 to 12 of the periodic table have been the focus of attention for the low-energy experimental research during the last 15 years. Unexpected experimental changes were found in friction when d electrons start to be active in the collisions. It can be thought of as an inhomogeneous r_S, depending on the impact velocity. However, even for the transition metals, those elements of groups 3 to 6 (the d subshells mostly empty) have canonical r_s values and could be tested by our nonperturbative model if low-energy stopping data were available. Some examples are V ($r_S = 1.66$) with no data for $E < 30$ keV, Nb ($r_S = 3.07$) with no data for $E < 20$ keV and great dispersion of the experimental data around the maximum of the sopping power, and Mo ($r_S = 1.61$) with no data for $E < 70$ keV. Even the relativistic W ($r_S = 1.62$) has no data for $E < 80$ keV. An interesting case is Ta, with very recent measurements for $E < 10$ keV by Roth *et al.* [45], and an unexplained high density of valence electrons. This target requires the relativistic treatment to determine the shell to shell electronic densities and binding energies for the SLPA calculation of the stopping by inner shells.

All the targets mentioned above are interesting aims for future experimental and theoretical research. Knowing their stopping values is important, not only as atomic solids but also because they are known partners in compounds of technological interest [24], and most of the stopping calculations in compounds are obtained from their components, with bond corrections in some cases. So reliable predictions of their values would be very useful.

V. CONCLUSIONS

In this paper we propose a nonlinear model to deal with low and intermediate impact stopping based on a central screened potential for a projectile moving in a free-electron gas. This potential induces a density of electrons that verifies the cusp condition at the origin, independently of the impact velocity, and the charge sign of the intruder.

In order to test this model for proton and antiproton impact we chose canonical solid targets (a reliable value of the Wigner-Seitz radius r_S), with experimental data available in the low-energy region: Cr, C, Be, Ti, Si, Al, Ge, Pb, and Li. The comparison at low impact velocities was done in terms of the friction (stopping power per impact velocity), which is

a very sensitive parameter, and allowed us to test the linear dependency with the velocity.

We proved that the present nonperturbative model gives a good description of the low-energy data for antiprotons in C, Si, and Al, and for protons in Cr, Be, Ti, Si, Al, Ge, and Pb. For protons in C and Li some small overestimation is found as discussed in the text.

By combining the present model for low to intermediate energies, and the dielectric formalism (including plasmons) for intermediate to high energies, a good description of the stopping power was obtained in an extended energy range. The inner-shell contribution was included by using the perturbative SLPA model. A detailed theoretical-experimental comparison was performed considering all the data available. We analyzed our results in three energy regions: for low impact energies up to that of plasmon excitations (the nonperturbative regime), for high energies (the perturbative regime), and in the intermediate-energy region. We showed that in this intermediate region the nonperturbative description and the plasmon excitation compete in importance, depending on the r_S. We suggested that the perturbative description is valid for $v/v_F \geqslant r_S\ Z_P$. However, we found that for $r_S < 2.1$ the perturbative results are valid even for lower impact velocities, $v/v_F \simeq 1.3\ Z_P$.

We recall the importance of Rb as a highly nonperturbative case (very low v_F) with no low-energy measurements. We have also detected at least 13 elements of well-known r_S but with unmeasured stopping power at low energies. These targets deserve future experimental and theoretical research.

ACKNOWLEDGMENTS

This paper was supported by the following institutions of Argentina: Consejo Nacional de Investigaciones Científicas y Técnicas, Agencia Nacional de Promoción Científica y Tecnológica, and Universidad de Buenos Aires. The authors acknowledge Pedro Grande for useful comments on this paper.

[1] Stopping Power of Matter for Ions, Graphs, Data, Comments and Programs, https://www-nds.iaea.org/stopping/.

[2] H. Bethe, Zur Theorie des durchgangs schneller Korpuskularstrahlen durch materie, Ann. Phys. **5**, 325 (1930).

[3] M. A. L. Marques and E. K. U. Gross, Time-dependent density functional theory, Annu. Rev. Phys. Chem. **55**, 427 (2004).

[4] M. Quijada, A. G. Borisov, I. Nagy, R. Díez Muiño, and P. M. Echenique, Time-dependent density-functional calculation of the stopping power for protons and antiprotons in metals, Phys. Rev. A **75**, 042902 (2007).

[5] A. A. Shukri, F. Bruneval, and L. Reining, *Ab initio* electronic stopping power of protons in bulk materials, Phys. Rev. B **93**, 035128 (2016).

[6] M. A. Zeb, J. Kohanoff, D. Sánchez-Portal, A. Arnau, J. I. Juaristi, and E. Artacho, Electronic Stopping Power in Gold: The Role of *d* Electrons and the H=He Anomaly, Phys. Rev. Lett. **108**, 225504 (2012).

[7] J. Lindhard, On the properties of a gas of charged particles, Mat. Fys. Medd. Dan. Vid. Selsk **28**, 1 (1954).

[8] J. Lindhard and A. Winter, Stopping power of electron gas and equipartition rule, Mat. Fys. Medd. Dan. Vid. Selsk **34**, 1 (1964).

[9] J. Lindhard and M. Scharff, Energy dissipation by ions in the kev region, Phys. Rev. **124**, 128 (1961).

[10] I. Abril, R. Garcia-Molina, C. D. Denton, F. J. Pérez-Pérez, and N. R. Arista, Dielectric description of wakes and stopping powers in solids, Phys. Rev. A **58**, 357 (1998).

[11] C. C. Montanari and J. E. Miraglia, *The Dielectric Formalism for Inelastic Processes in High-Energy Ion Matter Collisions*, Advanced Quantum Chemistry Vol. 65, edited by Dz. Belkic (Elsevier, Amsterdam, 2013), Chap. 7, pp. 165–201.

[12] C. C. Montanari, J. E. Miraglia, and N. R. Arista, Dynamics of solid inner-shell electrons in collisions with bare and dressed swift ions, Phys. Rev. A **66**, 042902 (2002).

[13] T. L. Ferrell and R. H. Ritchie, Energy losses by slow ions and atoms to electronic excitation in solids, Phys. Rev. B **16**, 115 (1977).

[14] P. M. Echenique, F. Flores, and R. H. Ritchie, Dynamic screening of ions in matter, Solid State Phys. **43**, 229 (1990).

[15] P. Sigmund and A. Schinner, Binary stopping theory for swift heavy ions, Eur. Phys. J. D **12**, 425 (2000).

[16] G. Schiwietz and P. L. Grande, A unitary convolution approximation for the impact-parameter dependent electronic energy loss, Nucl. Instrum. Methods Phys. Res. B **153**, 1 (1999); The unitary convolution approximation for heavy ions, **195**, 55 (2002).

[17] N. R. Arista, Energy loss of ions in solids: Non-linear calculations for slow and swift ions, Nucl. Instrum. Methods Phys. Res. B **195**, 91 (2002).

[18] J. J. Bailey, A. S. Kadyrov, I. B. Abdurakhmanov, D. V. Fursa, and I. Bray, Antiproton stopping in atomic targets, Phys. Rev. A **92**, 022707 (2015).

[19] J. F. Ziegler, M. D. Ziegler, and J. P. Biersack, SRIM: The stopping and range of ions in matter, Nucl. Instrum. Methods Phys. Res. B **268**, 1818 (2010); SRIM code, http://www.srim.org/.

[20] U. Fano, Penetration of protons, alpha particles, and mesons, Annu. Rev. Nucl. Sci. **13**, 1 (1963).

[21] M. Inokuti, Inelastic collisions of fast charged particles with atoms and molecules: The Bethe theory revisited, Rev. Mod. Phys. **43**, 297 (1971).

[22] N. R. Arista and A. F. Lifschitz, Non-linear approach to the energy loss of ions in solids, Adv. Quantum Chem. **45**, 47 (2004).

[23] P. Sigmund, Six decades of atomic collisions in solids, Nucl. Instrum. Methods Phys. Res. B (2017), doi:10.1016/j.nimb.2016.12.004.

[24] C. C. Montanari and P. Dimitrou, The IAEA stopping power database, following the trends in stopping power of ions in matter, Nucl. Instrum. Methods Phys. Res. B (2017), doi:10.1016/j.nimb.2017.03.138.

[25] E. Widmann, Plans for a next-generation low-energy antiproton facility, Phys. Scr. **72**, C51 (2005).

[26] Facility for Antiproton and Ion Research, http://www.fair-center.eu/.

[27] J. Allison *et al.*, Recent developments in Geant4, Nucl. Instrum. Methods Phys. Res. A **835**, 186 (2016).

[28] N. P. Barradas and E. Rauhala, Data analysis software for ion beam analysis, Joint ICTP/IAEA Workshop on Advanced Simulation and Modelling for Ion Beam Analysis, 2009 (2015), http://indico.ictp.it/event/a08139/session/4/contribution/3/material/0/1.pdf.

[29] International Commission on Radiation Units and Measurements, ICRU Report No. 37, Stopping Powers for Electrons and Positions (1984); ICRU Report No. 49, Stopping Power and Ranges for Protons and Alpha Particles (1993); ICRU Report No 73, Stopping of Ions Heavier Than Helium (2005).

[30] K. Wittmaack, On the origin of apparent Z1-oscillations in low-energy heavy-ion ranges, Nucl. Instrum. Methods Phys. Res. B **388**, 15 (2016).

[31] S. P. Møller, A. Csete, T. Ichioka, H. Knudsen, U. I. Uggerhoj, and H. H. Andersen, Stopping Power in Insulators and Metals without Charge Exchange, Phys. Rev. Lett. **93**, 042502 (2004).

[32] S. P. Møller, A. Csete, T. Ichioka, H. Knudsen, U. I. Uggerhøj, and H. H. Andersen, Antiproton Stopping at Low Energies: Confirmation of Velocity-Proportional Stopping Power, Phys. Rev. Lett. **88**, 193201 (2002).

[33] S. P. Møller, E. Uggerhøj, H. Bluhme, H. Knudsen, U. Mikkelsen, K. Paludan, and E. Morenzoni, Direct measurements of the stopping power for antiprotons of light and heavy targets, Phys. Rev. A **56**, 2930 (1997).

[34] J. E. Valdes, J. C. Eckardt, G. H. Lantschner, and N. R. Arista, Energy loss of slow protons in solids: Deviation from the proportionality with projectile velocity, Phys. Rev. A **49**, 1083 (1994).

[35] G. Hobler, K. K. Bourdelle, and T. Akatsu, Random and channeling stopping power of H in Si below 100 keV, Nucl. Instrum. Methods Phys. Res. B **242**, 617 (2006).

[36] M. Fama, G. H. Lantschner, J. C. Eckardt, N. R. Arista, J. E. Gayone, E. Sanchez, and F. Lovey, Energy loss and angular dispersion of 2200 keV protons in amorphous silicon, Nucl. Instrum. Methods Phys. Res. B **193**, 91 (2002).

[37] D. Roth, D. Goebl, D. Primetzhofer, and P. Bauer, A procedure to determine electronic energy loss from relative measurements with TOF-LEIS, Nucl. Instrum. Methods Phys. Res. B **317**, 61 (2013).

[38] D. Primetzhofer, S. Rund, D. Roth, D. Goebl, and P. Bauer, Electronic Excitations of Slow Ions in a Free Electron Gas Metal: Evidence for Charge Exchange Effects, Phys. Rev. Lett. **107**, 163201 (2011).

[39] E. A. Figueroa, E. D. Cantero, J. C. Eckardt, G. H. Lantschner, J. E. Valdés, and N. R. Arista, Threshold effect in the energy loss of slow protons and deuterons channeled in Au crystals, Phys. Rev. A **75**, 010901 (2007).

[40] E. D. Cantero, G. H. Lantschner, J. C. Eckardt, and N. R. Arista, Velocity dependence of the energy loss of very slow proton and deuteron beams in Cu and Ag, Phys. Rev. A **80**, 032904 (2009).

[41] S. N. Markin, D. Primetzhofer, M. Spitz, and P. Bauer, Electronic stopping of low-energy H and He in Cu and Au investigated by time-of-flight low-energy ion scattering, Phys. Rev. B **80**, 205105 (2009).

[42] D. Goebl, K. Khalal-Kouache, D. Roth, E. Steinbauer, and P. Bauer, Energy loss of low-energy ions in transmission and backscattering experiments, Phys. Rev. A **88**, 032901 (2013).

[43] D. Goebl, W. Roessler, D. Roth, and P. Bauer, Influence of the excitation threshold of d electrons on electronic stopping of slow light ions, Phys. Rev. A **90**, 042706 (2014).

[44] C. E. Celedon, E. A. Sanchez, L. Salazar Alarcon, J. Guimpel, A. Cortes, P. Vargas, and N. R. Arista *et al.*, Band structure effects in the energy loss of low-energy protons and deuterons in thin films of Pt, Nucl. Instrum. Methods Phys. Res. B **360**, 103 (2015).

[45] D. Roth, B. Bruckner, M. V. Moro, S. Gruber, D. Goebl, J. I. Juaristi, M. Alducin, R. Steinberger, J. Duchoslav, D. Primetzhofer, and P. Bauer, Electronic Stopping of Slow Protons in Transition and Rare Earth Metals: Breakdown of the Free Electron Gas Concept, Phys. Rev. Lett. **118**, 103401 (2017).

[46] P. M. Echenique, R. M. Nieminen, and R. H. Ritchie, Density functional calculation of stopping power of an electron gas for slow ions, Solid State Commun. **37**, 779 (1981).

[47] E. Zaremba, A. Arnau, and P. M. Echenique, Nonlinear screening and stopping powers at finite projectile velocities, Nucl. Instrum. Methods Phys. Res. B **96**, 619 (1995).

[48] I. Nagy and B. Apagyi, Scattering-theory formulation of stopping powers of a solid target for protons and antiprotons with velocity-dependent screening, Phys. Rev. A **58**, R1653 (1998).

[49] I. Nagy and A. Bergara, A model for the velocity-dependent screening, Nucl. Instrum. Methods Phys. Res. B **115**, 58 (1996).

[50] I. Nagy, Low-velocity antiproton stopping, A trial-potential approach, Nucl. Instrum. Methods Phys. Res. B **94**, 377 (1994).

[51] A. F. Lifschitz and N. R. Arista, Electronic energy loss of helium ions in aluminum using the extended-sum-rule method, Phys. Rev. A **58**, 2168 (1998).

[52] J. M. Fernández-Varea, and N. R. Arista, Analytical formula for the stopping power of low-energy ions in a free-electron gas, Radiat. Phys. Chem. **96**, 88 (2014).

[53] H. B. Nersisyan, J. M. Fernández-Varea, and N. R. Arista, Dynamic screening of an ion in a degenerate electron gas within the second-order Born approximation, Nucl. Instrum. Methods Phys. Res. B **354**, 167 (2015).

[54] R. Cabrera-Trujillo, Y. Öhrn, E. Deumens, and J. R. Sabin, Stopping cross section in the low- to intermediate-energy range: Study of proton and hydrogen atom collisions with atomic N, O, and F, Phys. Rev. A **62**, 052714 (2000).

[55] J. J. Bailey, A. S. Kadyrov, I. B. Abdurakhmanov, D. V. Fursa, and I. Bray, Antiproton stopping in H_2 and H_2O, Phys. Rev. A **92**, 052711 (2015).

[56] P. L. Grande, Alternative treatment for the energy-transfer and transport cross section in dressed electron-ion binary collisions, Phys. Rev. A **94**, 042704 (2016).

[57] D. Isaacson, *Compilation of rs Values*, New York University Rept. No. 02698 (National Auxiliary Publication Service, New York, 1975).

[58] K. S. Singwi, M. O. Tosi, R. H. Land, and A. Sjölander, Electron correlations at metallic densities, Phys. Rev. **176**, 589 (1968).

[59] E. D. Cantero, R. C. Fadanelli, C. C. Montanari, M. Behar, J. C. Eckardt, G. H. Lantschner, J. E. Miraglia, and N. R. Arista, Experimental and theoretical study of the energy loss of Be and B ions in Zn, Phys. Rev. A **79**, 042904 (2009).

[60] C. C. Montanari, C. D. Archubi, D. M. Mitnik, and J. E. Miraglia, Energy loss of protons in Au, Pb, and Bi using relativistic wave functions, Phys. Rev. A **79**, 032903 (2009).

[61] I. Nagy and P. M. Echenique, Stopping power of an electron gas for antiprotons at intermediate velocities, Phys. Rev. A **47**, 3050 (1993).
[62] C. C. Montanari, J. E. Miraglia, and N. R. Arista, Suppression of projectile-electron excitations in collisions with a free-electron gas of metals, Phys. Rev. A **62**, 052902 (2000).
[63] E. Fermi and E. Teller, Capture of negative mesotrons in matter, Phys. Rev. **72**, 399 (1947).
[64] http://www.fair-center.eu/public/experiment-program/appa-physics/flair.html; http://www.flairatfair.eu/.
[65] P. Sigmund, *Particle Penetration and Radiation Effects, General Aspects and Stopping of Swift Point Charges* (Springer-Verlag, Berlin, 2006), Vol. 1.
[66] C. F. Bunge, J. A. Barrientos, A. V. Bunge, and J. A. Cogordan, Hartree-Fock and Roothaan-Hartree-Fock energies for the ground states of He through Xe, Phys. Rev. A **46**, 3691 (1992).
[67] S. P. Limandri *et al.*, Stopping cross sections of TiO_2 for H and He ions, Eur. Phys. J. D **68**, 194 (2014).
[68] R. C. Fadanelli, C. D. Nascimento, C. C. Montanari, J. C. Aguiar, D. Mitnik, A. Turos, E. Guziewicz, and M. Behar, Stopping and straggling of H and He in ZnO, Eur. Phys. J. D **70**, 178 (2016).
[69] G. P. Williams, *Electron Binding Energies of the Elements*, CRC Handbook of Chemistry and Physics Vol. F170 (CRC, Boca Raton, 1986); http://www.jlab.org/gwyn/ebindene.html.
[70] Ch. Eppacher and D. Semrad, Dependence of proton and helium energy loss in solids upon plasma properties, Nucl. Instrum. Methods Phys. Res. B **69**, 33 (1992).
[71] S. D. Warshaw, The stopping power for protons in several metals, Phys. Rev. **76**, 1759 (1949).
[72] D. Kahn, The energy loss of protons in metallic foils and mica, Phys. Rev. **90**, 503 (1953).
[73] E. P. Arkhipov and Y. V. Gott, Slowing down of 0.5-30 keV protons in some materials, Sov. Phys. JETP **29**, 615 (1969).
[74] J. H. Ormrod, Electronic stopping cross sections of deutrons in titanium, Nucl. Instrum. Methods **95**, 49 (1971).
[75] M. Abdesselam, S. Ouichaoui, M. Azzouz, A. C. Chami, and M. Siad, Stopping of 0.3–1.2 MeV/u protons and alpha particles in Si, Nucl. Instrum. Methods Phys. Res. B **266**, 3899 (2008).
[76] G. Konac, S. Kalbitzer, C. Klatt, D. Niemann, and R. Stoll, Energy loss and straggling of H and He ions of keV energies in Si and C, Nucl. Instrum. Methods Phys. Res. B **136–138**, 159 (1998).
[77] C. D. Archubi and N. R. Arista, A study of threshold effects in the energy loss of slow protons in semiconductors and insulators using dielectric and non-linear approaches, Eur. Phys. J. B **89**, 86 (2016).
[78] R. Ullah, F. Corsetti, D. Sánchez-Portal, and E. Artacho, Electronic stopping power in a narrow band gap semiconductor from first principles, Phys. Rev. B **91**, 125203 (2015).
[79] T. Kaneko, Partial and total electronic stopping cross sections of atoms and solids for protons, At. Data Nucl. Data Tables **53**, 271 (1993).
[80] R. Cabrera-Trujillo, J. R. Sabin, E. Deumens, and Y. Ohrn, Cross sections for H^+ and H atoms colliding with Li in the low-keV-energy region, Phys. Rev. A **78**, 012707 (2008).
[81] C. Eppacher, R. Diez Muino, D. Semrad, and A. Arnau, Stopping power of lithium for hydrogen projectiles, Nucl. Instrum. Methods Phys. Res. B **96**, 639 (1995).